

## Enhanced visible-light-driven photocatalytic activity of $\text{Ag}_2\text{WO}_4/\text{g-C}_3\text{N}_4$ heterojunction photocatalysts for tetracycline degradation

Yu Shi<sup>a</sup>, Yu-bin Tang<sup>a,\*</sup>, Fang-yan Chen<sup>a,\*</sup>, Wei-long Shi<sup>b</sup>, Feng Guo<sup>c</sup>, Xin-gang Wang<sup>a</sup>

<sup>a</sup>School of Environmental and Chemical Engineering, Jiangsu University of Science and Technology, Zhenjiang, Jiangsu 212003, China, Tel. +86-511-84448601; email: ybill@163.com (Y.-b. Tang), Tel. +86-511-85605157; emails: catchen1029@sohu.com (F.-y. Chen), 291197172@qq.com (Y. Shi), hofs@163.com (X.-g. Wang)

<sup>b</sup>School of Material Science and Engineering, Jiangsu University of Science and Technology, Zhenjiang, Jiangsu 212003, China, Tel. +86-511-85605157; email: shiwl@just.edu.cn

<sup>c</sup>School of Energy and Power Engineering, Jiangsu University of Science and Technology, Zhenjiang, Jiangsu 212003, China, Tel. +86-511-85605157; email: gfeng0105@126.com

Received 26 February 2019; Accepted 26 July 2019

### ABSTRACT

Heterogeneous photocatalysis has become one of the most potential technologies due to its ability to alleviate energy shortages and environmental pollution. In this work, a heterojunction photocatalyst of  $\text{Ag}_2\text{WO}_4/\text{g-C}_3\text{N}_4$  was synthesized via simple deposition method. The as-prepared samples were characterized by SEM, HRTEM, X-ray photoelectron spectroscopy, UV-vis, photoluminescence, and photocurrent measurements. The photocatalytic performance of the heterojunction photocatalyst for the degradation of tetracycline under visible light was investigated. It is demonstrated in our experiment that by loading a small amount of  $\text{Ag}_2\text{WO}_4$  nanoparticles onto  $\text{g-C}_3\text{N}_4$ , the photocatalytic activity can be improved for tetracycline degradation. The as-prepared heterojunctions have fast interfacial charge transfer speed and exhibit enhanced visible-light-driven photocatalytic activity for tetracycline degradation. Under the irradiation of visible light, the photocatalytic degradation efficiency of TC (tetracycline) by using  $\text{Ag}_2\text{WO}_4/\text{g-C}_3\text{N}_4$  heterojunction (3AW-CN) prepared under optimized conditions is 1.08 and 0.63 times higher than that by using pure  $\text{g-C}_3\text{N}_4$  and pure  $\text{Ag}_2\text{WO}_4$ , respectively. The significantly enhanced photocatalytic activity is mainly due to the fact that silver nanoparticles could act as reservoirs and donors for electrons, thereby effectively regulating electron transfer and promoting charge separation.

**Keywords:**  $\text{Ag}_2\text{WO}_4$ ;  $\text{g-C}_3\text{N}_4$ ; Heterojunction; Tetracycline; Photocatalyst

### 1. Introduction

As a common antibiotic, TC is widely used in the medical and aquaculture industries [1]. In recent years, due to the abuse of antibiotics and the arbitrary discharge of wastewater from pharmaceutical enterprises, antibiotics and their derivatives remained in water and food, and eventually enriched through the food chains, which has negative impact on human health [2,3]. Therefore, an

environmentally friendly method with high-efficiency and low-cost consideration is desperately needed to remove the tetracycline in water. Among many methods, the semiconductor photocatalysts have attracted great attention for the ability to effectively degrade the target pollutants under sunlight. It is well known that visible light accounts for about 42%–45% of sunlight [4,5], while ultraviolet radiation accounting for only about 5% of the total solar radiation [6,7]. So, it is meaningful to develop cheap and highly

\* Corresponding authors.

efficient visible-light responsive photocatalysts to remove tetracycline from wastewater.

In recent years, many reported works have proposed various types of photocatalysts, including metal oxides [8–10], metal sulfides [11,12], halides [13,14], molybdates [15], tungstates [16,17], non-metallic catalysts [18–20], and so on. Graphite-like carbon nitride ( $g\text{-C}_3\text{N}_4$ ) has attracted much attention as an important non-metallic semiconductor material with a band gap of about 2.70 eV, which shows a possession of photocatalytic activity under visible-light irradiation. Meanwhile,  $g\text{-C}_3\text{N}_4$  possesses the characteristics of 2D layered structure, and performs strong thermal and chemical stability. Moreover, it is not susceptible to photocorrosion under illumination [21,22]. However, the catalytic activity of  $g\text{-C}_3\text{N}_4$  is limited due to its weak light absorption capacity and fast recombination of photoelectron–hole pairs.

Therefore, in order to effectively solve the above problems, the bulk phase  $g\text{-C}_3\text{N}_4$  needs to be modified, such as constructing a heterojunction semiconductor, doping a noble metal element, introducing a promoter, and so forth. Among these methods, heterojunction semiconductor construction method [23–25] can effectively regulate the energy band structure of  $g\text{-C}_3\text{N}_4$  and strongly inhibit the recombination of photogenerated carriers, thus improving the photocatalytic activity of the photocatalysts to pollutants and increasing the degradation rate. It has been proved to be a simple and feasible modification method. For example, Xia et al. [26] has fabricated a direct Z-scheme heterojunction  $g\text{-C}_3\text{N}_4/\text{MnO}_2$  by using solution deposition method. The combination of photoelectrons in the valence band of  $\text{MnO}_2$  and holes in the conduction band of  $g\text{-C}_3\text{N}_4$  under light excitation leads to an improvement of the charge carriers generation and utilization, and improves the photocatalytic efficiency [26]. Some reported works have synthesized semiconductor catalysts by combining Ag compounds or simple substance silver with  $g\text{-C}_3\text{N}_4$ , such as  $\text{Ag}_2\text{SO}_4$  [27],  $\text{Ag}_2\text{CrO}_4$  [28],  $\text{Ag}_2\text{SO}_3$  [29] and Ag [30–32] were combined with  $g\text{-C}_3\text{N}_4$ . He et al. [33] synthesized  $\text{Ag}_3\text{PO}_4/g\text{-C}_3\text{N}_4$  for the first time by in situ precipitation method, which convert  $\text{CO}_2$  into fuel under simulated solar irradiation. It was found that the heterojunction structure formed by  $\text{Ag}_3\text{PO}_4$  and  $g\text{-C}_3\text{N}_4$ , effectively promoted the separation of electron–hole pairs through Z-scheme mechanism, and ultimately improved the photocatalytic performance of  $\text{Ag}_3\text{PO}_4/g\text{-C}_3\text{N}_4$  for  $\text{CO}_2$  reduction [33]. Ong et al. [34] loaded active silver halide  $\text{AgX}$  ( $X = \text{Cl}, \text{Br}$ ) on protonated graphite carbon nitride (pCN) by ultrasonic assisted deposition. Based on the experiment results, an enhancement of photocatalytic activity is observed due to the synergy of the surface plasmon resonance (SPR) effect of silver and the heterojunction structure formed by pCN and AgBr, so that the charge can be transferred and separated quickly, avoiding recombination. Motivated by the above works, we proposed a method of construction of heterojunctions with Ag-based compounds and  $g\text{-C}_3\text{N}_4$  to separate photogenerated electrons and holes efficiently, inhibit charge recombination, and thereby improve heterojunction photocatalytic activity.

$\text{Ag}_2\text{WO}_4$  is a common Ag-based compound with a band gap of about 3.10 eV, which means a suitable valence band and conduction band position. According to the empirical

formula:  $E_{\text{VB}} = X - E_c + 1/2 E_g$  [35], the energy at the bottom of the conduction band and the top of the valence band can be calculated to be about  $-0.03$  and  $3.00$  eV, respectively. Thus, the more positive conduction band position of  $\text{Ag}_2\text{WO}_4$  can accept electrons from the  $g\text{-C}_3\text{N}_4$  conduction band, thereby promoting photocatalytic reaction. In previous reported works, Dai et al. [36] prepared  $\text{Ag}_2\text{WO}_4/g\text{-C}_3\text{N}_4$  photocatalysts by a complex method which combines precipitation and hydrothermal processes. In the photocatalyst preparation process, they have demonstrated that the mass ratio of  $\text{Ag}_2\text{WO}_4$  to  $g\text{-C}_3\text{N}_4$  was large, and even reached 60%. Jiang et al. [37] prepared  $\alpha\text{-Ag}_2\text{WO}_4/g\text{-C}_3\text{N}_4$  photocatalyst with a complicated three-step method. The  $\alpha\text{-Ag}_2\text{WO}_4$  is synthesized in two steps, namely precipitation and hydrothermal processes, and then  $\alpha\text{-Ag}_2\text{WO}_4/g\text{-C}_3\text{N}_4$  photocatalyst is prepared with high temperature calcination. Previous work often used these complex methods to prepare photocatalysts with a high mass ratio of  $\text{Ag}_2\text{WO}_4$  to  $g\text{-C}_3\text{N}_4$ , which would limit the practical application of the photocatalyst.

However, Ag is a precious metal; high level Ag doping will cause a significant increase in the cost of the photocatalyst preparation, which is unfavourable to the wide application of the catalyst. Therefore, in this work, small amount of  $\text{Ag}_2\text{WO}_4$  and  $g\text{-C}_3\text{N}_4$  were combined by in situ precipitation method to form the  $\text{Ag}_2\text{WO}_4/g\text{-C}_3\text{N}_4$  heterojunction photocatalyst, which can not only improve the photocatalytic degradation performance of  $g\text{-C}_3\text{N}_4$ , but also lower the cost for industrial production.

## 2. Experimental section

### 2.1. Synthesis of pure $g\text{-C}_3\text{N}_4$ powder

Pure  $g\text{-C}_3\text{N}_4$  powders were prepared by calcination method [38,39]. 5 g dicyandiamide was weighed and placed in an alumina crucible with cover, calcined in a muffle furnace for 4 h at  $550^\circ\text{C}$ , the heating rate is  $2.3^\circ\text{C}/\text{min}$ , then naturally cooled down to room temperature, and ground to obtain pale yellow  $g\text{-C}_3\text{N}_4$  powders.

### 2.2. Synthesis of $\text{Ag}_2\text{WO}_4/g\text{-C}_3\text{N}_4$ (AW-CN)

$\text{Ag}_2\text{WO}_4/g\text{-C}_3\text{N}_4$  (AW-CN) was prepared by the in situ co-precipitation method [40,41]. In a typical case, 0.334 g of pure  $g\text{-C}_3\text{N}_4$  powder was added into 50 mL distilled water with proper stirring, and then successively mixed with 10 mL of 7.59 mmol/L  $\text{AgNO}_3$  solutions and 10 mL of 3.80 mmol/L  $\text{Na}_2\text{WO}_4$  solution with the same stir rate of 500 rpm for 0.5 h and 4 h at room temperature, respectively. The obtained precipitate was washed by distilled water and absolute ethanol for three times, and then dried in a vacuum oven at  $25^\circ\text{C}$  to obtain the sample with  $\text{Ag}_2\text{WO}_4$  mass fraction of 5%.

$\text{Ag}_2\text{WO}_4/g\text{-C}_3\text{N}_4$  sample which contains 1%, 3%, 5%, 7%, and 9%  $\text{Ag}_2\text{WO}_4$  was marked as 1AW-CN, 3AW-CN, 5AW-CN, 7AW-CN, and 9AW-CN, respectively. Pure  $\text{Ag}_2\text{WO}_4$  was prepared by the above method without adding  $g\text{-C}_3\text{N}_4$ .

## 3. Results and discussion

Fig. 1 shows the X-ray diffraction patterns of pure  $g\text{-C}_3\text{N}_4$ , 3AW-CN and pure  $\text{Ag}_2\text{WO}_4$ .

All diffraction peaks in the XRD pattern (trace b in Fig. 1) are assigned to the  $\text{Ag}_2\text{WO}_4$ , which is consistent with the values in the standard JCPDS card number (PDF #34-0061) of trace a. Both trace c and d show a strong diffraction peak at  $27.3^\circ$  which corresponds to the (002) plane reflection of the long-range in-plane stack for the  $\text{g-C}_3\text{N}_4$  conjugated aromatic

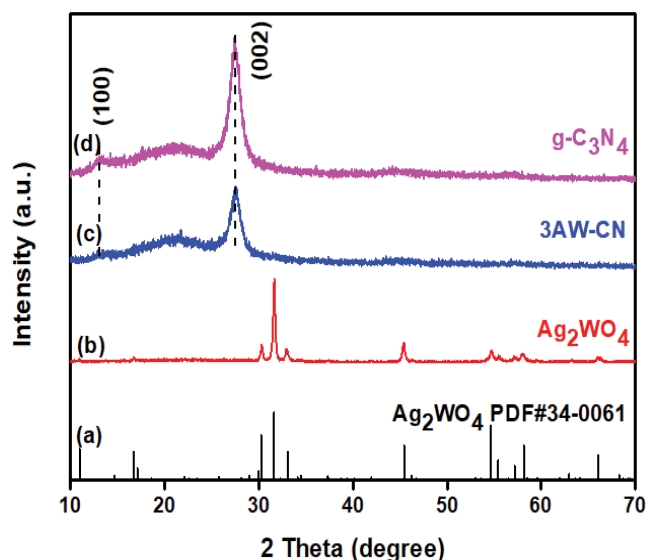


Fig. 1. Standard diffraction for  $\text{Ag}_2\text{WO}_4$  (PDF# 34-0061) (a), XRD patterns of pure  $\text{Ag}_2\text{WO}_4$  (b), 3AW-CN (c) and pure  $\text{g-C}_3\text{N}_4$  (d).

unit (JCPDS #87-1526), and the result is similar to the previous report [42]. There is no obvious  $\text{Ag}_2\text{WO}_4$  diffraction peak shown in trace c. This is because the mass ratio of  $\text{Ag}_2\text{WO}_4$  to  $\text{g-C}_3\text{N}_4$  in the 3AW-CN composite photocatalyst is only 3%. Besides, the relevant diffraction peaks are not detected, indicating that the crystal structure of  $\text{g-C}_3\text{N}_4$  is well maintained during the synthesis process.

Fig. 2 shows the SEM images of pure  $\text{g-C}_3\text{N}_4$ , pure  $\text{Ag}_2\text{WO}_4$  and 3AW-CN composites.

It is from Fig. 2a that the bulk  $\text{g-C}_3\text{N}_4$  is composed of thick sheet structure stacks with smooth surface and non-uniform size, but without fixed morphology. As shown in Fig. 2b, pure  $\text{Ag}_2\text{WO}_4$  exhibits a regular nanorod shape, which can facilitate sufficient contact with  $\text{g-C}_3\text{N}_4$  and increase the transport interface of photogenerated charge. When  $\text{Ag}_2\text{WO}_4$  is deposited on  $\text{g-C}_3\text{N}_4$  to form a heterojunction photocatalyst, such as 3AW-CN (Figs. 2c–d), it is clear that the introduction of a small amount of  $\text{Ag}_2\text{WO}_4$  do not change the overall morphology structure of  $\text{g-C}_3\text{N}_4$ .

Fig. 3a depicts the TEM image of 3AW-CN,  $\text{Ag}_2\text{WO}_4$  is anchored on the  $\text{g-C}_3\text{N}_4$  lamellar structure.  $\text{Ag}_2\text{WO}_4$  is compounded with  $\text{g-C}_3\text{N}_4$  by simple deposition method and deposited randomly on the  $\text{g-C}_3\text{N}_4$  lamella without agglomeration. The particle size of  $\text{Ag}_2\text{WO}_4$  is about 10–20 nm, as shown as the black spot in circle in Fig. 3a. Moreover, the mapping images of elements in the composite heterojunction photocatalyst show that C, N, Ag, W, and O are uniformly distributed in the HAADF-STEM images (Figs. 3b–g), and the formation of the composite heterojunction are determined.

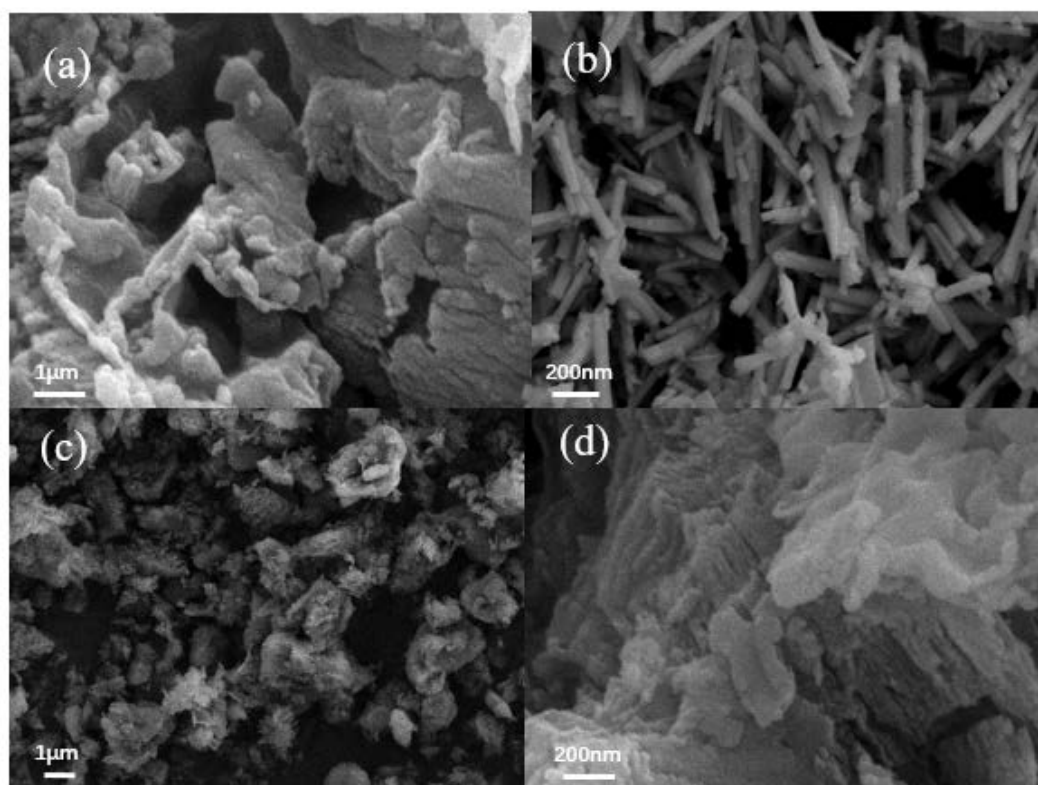


Fig. 2. SEM images of pure  $\text{g-C}_3\text{N}_4$  (a), pure  $\text{Ag}_2\text{WO}_4$  (b) and 3AW-CN (c, d).

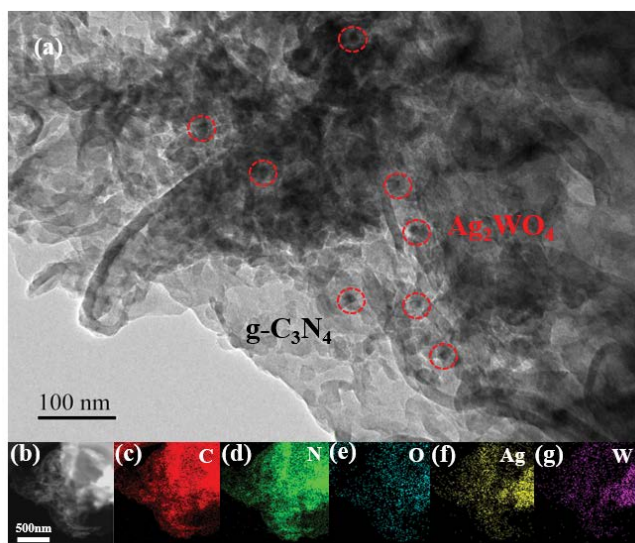


Fig. 3. HRTEM images (a), HAADF-STEM (b) and the corresponding elemental mapping images of 3AW-CN (c–g).

X-ray photoelectron spectroscopy (XPS) is used to analyze the elemental composition and chemical state of the sample. As shown in Fig. 4a, it is clearly shown that 3AW-CN consists of C, N, O, Ag, and W. Fig. 4b shows the C 1s spectrum with two different peaks at 284.6 and 288.1 eV. The first peak corresponds to graphitic carbon, and the second peak is derived from a carbon atom bonded with three nitrogen atoms in the  $g\text{-C}_3\text{N}_4$  lattice [43]. As shown in Fig. 4c, the N 1s XPS spectra can be divided into four peaks, the center of these peaks locates at 398.5, 399.5, 401.0, and 404.1 eV, respectively. The peak at 399.5 eV is attributed to the  $sp^3$  hybridized nitrogen atom ( $\text{N}(\text{-C})_3$ ), and the peak at 401.0 eV is attributed to the amino functional group containing a hydrogen atom (CNH) [44], and the  $\pi$ -excitation peak is located at 404.1 eV [45]. The XPS spectrum of O 1s in Fig. 4d can be divided into two peaks with binding energy of 530.3 and 532.2 eV, respectively, derived from OH groups, oxygen in adsorbed water or oxygen in  $\text{Ag}_2\text{WO}_4$  [46,47]. In Fig. 4e, two peaks center locate at the binding energy of 368.1 and 374.2 eV belong to Ag 3d<sub>5/2</sub> and Ag 3d<sub>3/2</sub>, respectively [36]. As shown in Fig. 4f, two peaks at 35.1 and 37.2 eV correspond to W 4f spectrum. We also analyze the XPS spectrum of Ag 3d in the 3AW-CN sample after one experiment, as shown in Fig. S1. The peaks at 368.3 and 374.4 eV correspond to Ag nanoparticles, which are derived from  $\text{Ag}_2\text{WO}_4$  photodecomposition [37]. All of the above analysis confirmed the successful synthesis of the  $\text{Ag}_2\text{WO}_4/g\text{-C}_3\text{N}_4$  composite.

At present research, the photocatalytic activity of the prepared photocatalyst is evaluated by measuring the degradation rate of TC under visible-light irradiation ( $\lambda > 420$  nm). The concentrations of TC aqueous solutions and photocatalysts dosage are fixed at 10 mg/L and 0.5 g/L, respectively. As shown in Fig. 5, the self-degradation of TC is negligible in the absence of any photocatalyst. It is noteworthy that the photocatalytic degradation efficiencies of TC by all the  $\text{Ag}_2\text{WO}_4/g\text{-C}_3\text{N}_4$  heterojunction photocatalysts containing various quantities of  $\text{Ag}_2\text{WO}_4$  are better than that by pure  $g\text{-C}_3\text{N}_4$  or pure  $\text{Ag}_2\text{WO}_4$  under the condition of 180 min

visible-light irradiation, indicating that the introduction of  $\text{Ag}_2\text{WO}_4$  significantly improved photocatalytic activity of  $g\text{-C}_3\text{N}_4$ . In detail, the photocatalytic degradation activity of 3%  $\text{Ag}_2\text{WO}_4/g\text{-C}_3\text{N}_4$  (3AW-CN) for TC is excellent, and the degradation efficiency of TC by 3AW-CN reached 76.9%, which is much better than that by pure  $g\text{-C}_3\text{N}_4$  (36.8%).

In order to study the optical properties of the as-prepared photocatalysts, the UV–Vis diffuse reflectance spectra of  $g\text{-C}_3\text{N}_4$ ,  $\text{Ag}_2\text{WO}_4$  and 3AW-CN are measured, as shown in Fig. 6a.

As depicted in Fig. 6a, 3AW-CN exhibits stronger absorption in ultraviolet and visible light region than pure  $g\text{-C}_3\text{N}_4$  does, which is consistent with the experimental results the photocatalytic degradation TC. And the band gap energy of  $\text{Ag}_2\text{WO}_4$  (Fig. 6b, the red trace) is calculated to be 3.07 eV based on the curve of  $(\alpha h\nu)^{0.5}$  vs.  $h\nu$ , which agrees with the previous reports [48]. For pure  $g\text{-C}_3\text{N}_4$ , a visible absorption edge appears around 460 nm with an estimated band gap of 2.70 eV (Fig. 6b, the black trace). After  $g\text{-C}_3\text{N}_4$  is combined with  $\text{Ag}_2\text{WO}_4$ , the absorption of 3AW-CN in the visible-light region was significantly increased compared with pure  $g\text{-C}_3\text{N}_4$ .

The PL spectrum reflects the recombination rate of photoexcited carriers [49]. Generally, the high PL emission peak indicates the high recombination rate of charge carriers. As shown in Fig. 7, pure  $g\text{-C}_3\text{N}_4$  shows a strong PL emission peak at 468 nm, indicating that the recombination of electrons and holes is rapid, while the PL signal of 3AW-CN significantly weakened under the same condition. Clearly, PL spectra demonstrates that the presence of  $\text{Ag}_2\text{WO}_4$  in AW-CN significantly impede the recombination of photoinduced electrons and holes.

Stability is an important factor for the evaluation of high-quality photocatalysts. At present study, the stability of 3AW-CN was investigated by cyclic photocatalytic degradation experiments of TC (Fig. 8a). It is found that 3AW-CN can still maintain excellent photocatalytic performance after five cycle experiments, indicating that 3AW-CN has excellent cyclic stability.

In order to study the possible mechanism of the photocatalytic degradation of TC by the prepared  $\text{Ag}_2\text{WO}_4/g\text{-C}_3\text{N}_4$  photocatalyst, the active species trapping experiment was carried out, as shown in Fig. 8b. As can be seen from Fig. 8b, the addition of Vc as an  $\text{O}_2^-$  radical scavenger, caused the most obvious decrease of the photocatalytic degradation efficiency of TC by using 3AW-CN. The results indicate that  $\text{O}_2^-$  plays the most important role in the photocatalytic degradation process. It can also be observed that the photogenerated holes improve the photocatalytic degradation of TC.

The separation efficiency of photogenerated electron–hole pairs is further confirmed by the photocurrent response and electrochemical impedance spectroscopy of the samples. On the one hand, the photocurrent density produced by 3AW-CN is significantly stronger than that by  $g\text{-C}_3\text{N}_4$  (Fig. 9a). On the other hand, the radius of the arc on the EIS Nyquist diagram of 3AW-CN electrode is obviously smaller than that of  $g\text{-C}_3\text{N}_4$  electrode (Fig. 9b). These results indicate that the separation efficiency of photogenerated electron–hole pair induced by 3AW-CN is higher than that by pure  $g\text{-C}_3\text{N}_4$ , which is consistent with the PL spectra.

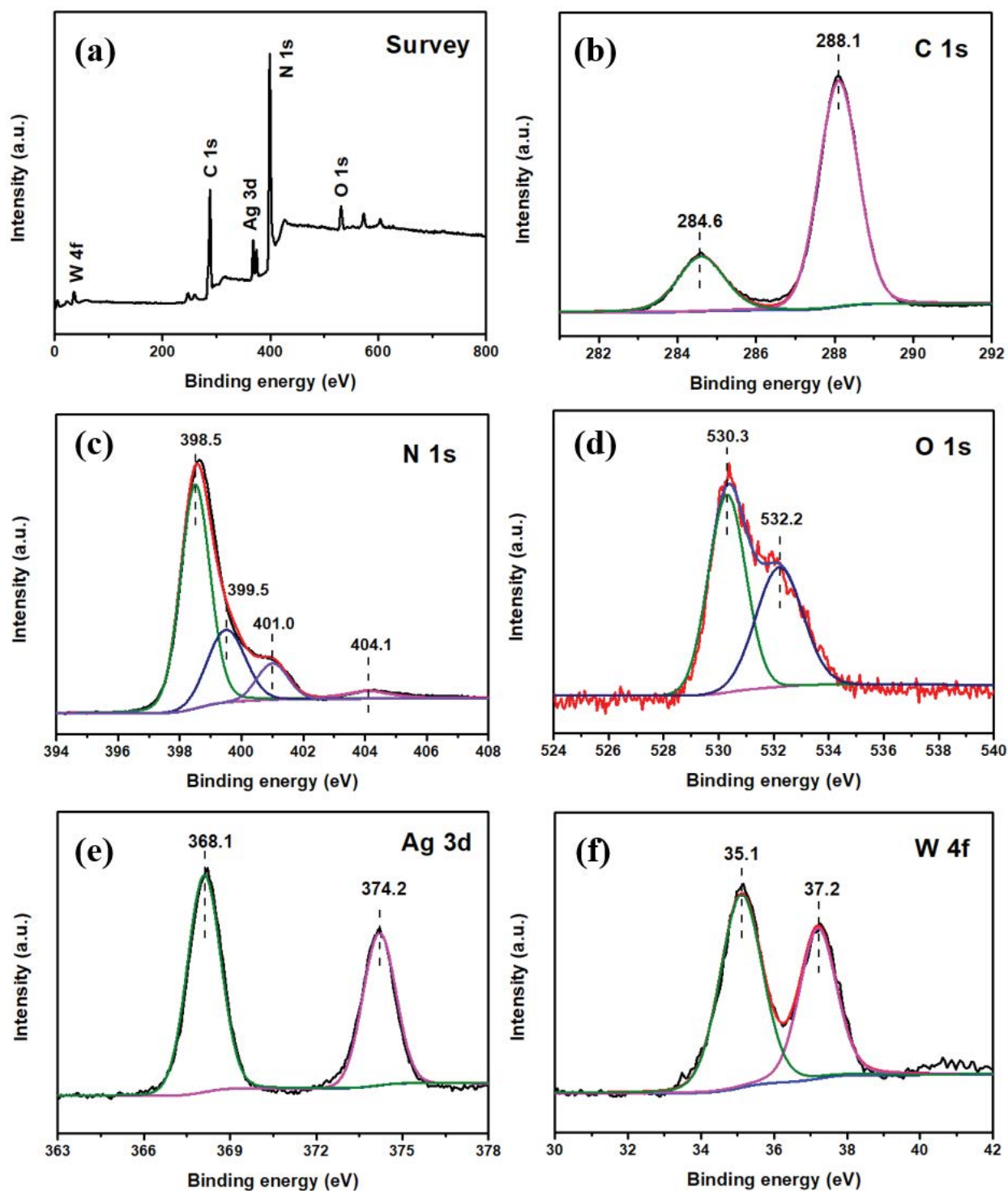


Fig. 4. XPS spectra of g-C<sub>3</sub>N<sub>4</sub> and 3AW-CN: survey of the sample (a), C 1s (b), N 1s (c), O 1s (d), Ag 3d (e), W 4f (f).

At present study, TOC was detected to evaluate the mineralization efficiency of TC. As shown in Fig. 10, it is clear that only 13.4% of TOC removal efficiency is observed by using pure g-C<sub>3</sub>N<sub>4</sub> sample. However, when the 3AW-CN sample was used, the TOC removal efficiency reaches 39.4%, indicating that TC was more easily to be mineralized by

3AW-CN, rather than by pure g-C<sub>3</sub>N<sub>4</sub>. This result is similar to the previous work [50].

Based on the above results, the excellent photocatalytic activity of 3AW-CN can be attributed to two aspects, that is, the increase of visible-light absorption and improvement of separation efficiency of photogenerated electron-hole pairs.

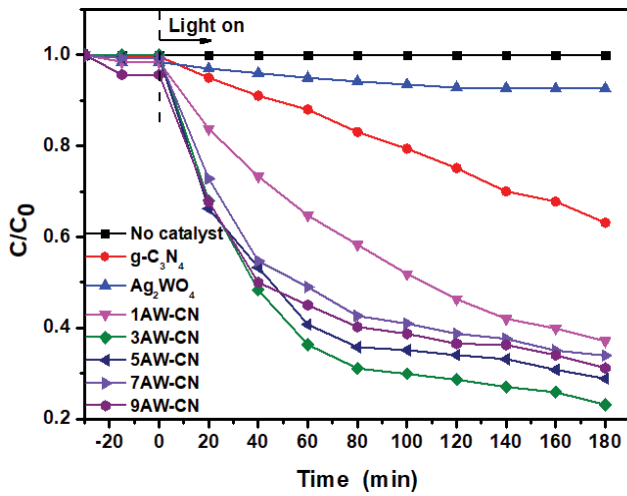


Fig. 5. Photocatalytic activity of the as-prepared photocatalysts toward the degradation of TC.

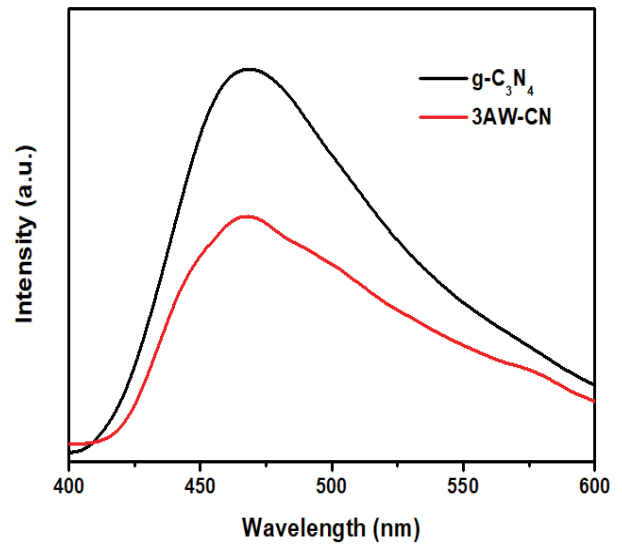


Fig. 7. PL spectra of  $g-C_3N_4$  and 3AW-CN.

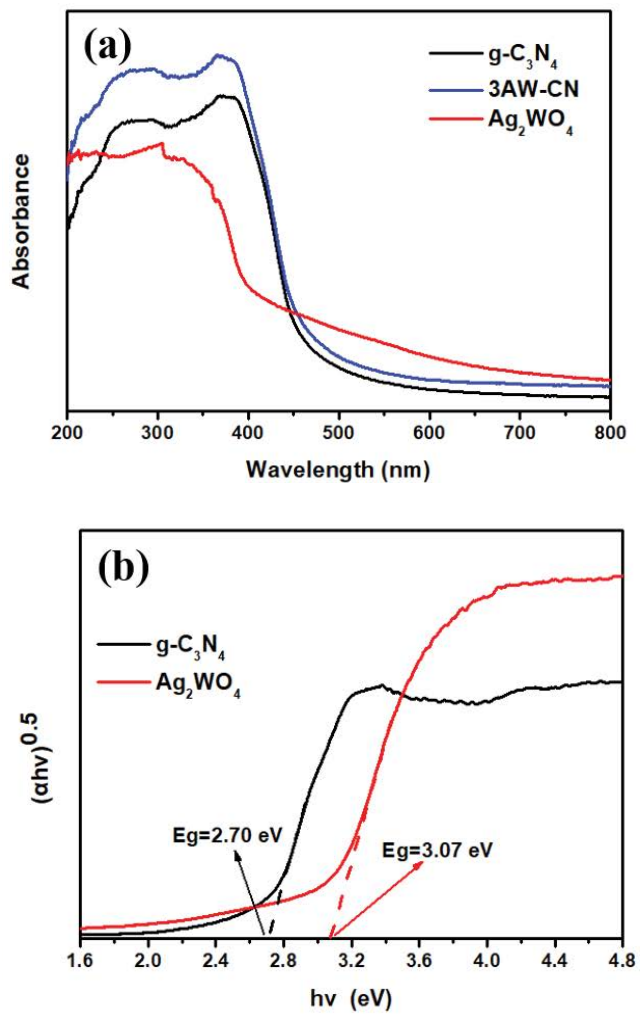


Fig. 6. UV-Vis diffuse reflectance spectra (a) and band gap energy of  $g-C_3N_4$  and the 3AW-CN (b).

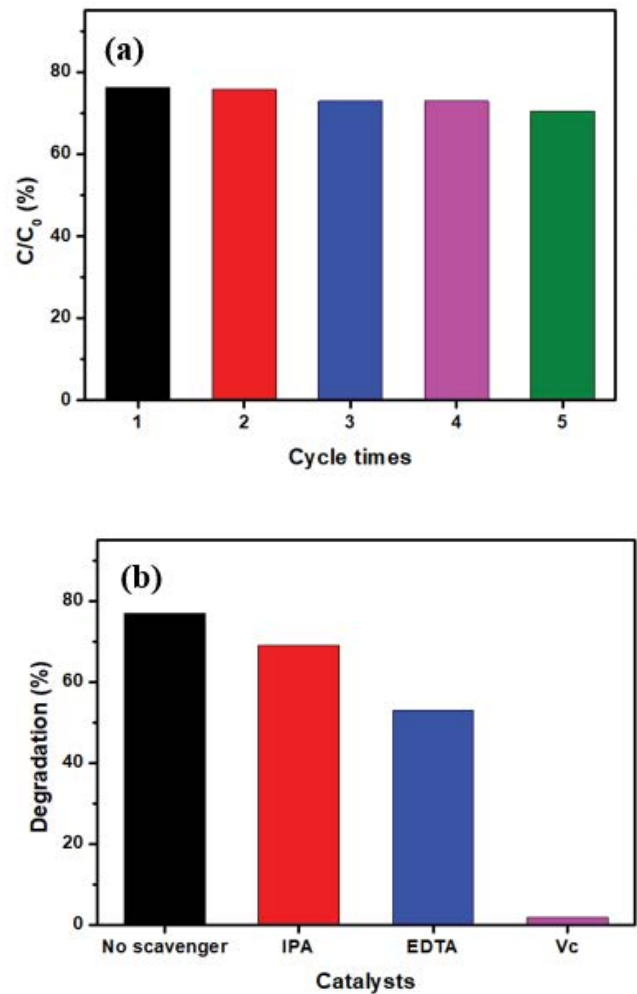


Fig. 8. Cycling test (a) and reactive-species-trapping experiments of 3AW-CN under visible light irradiation (b).

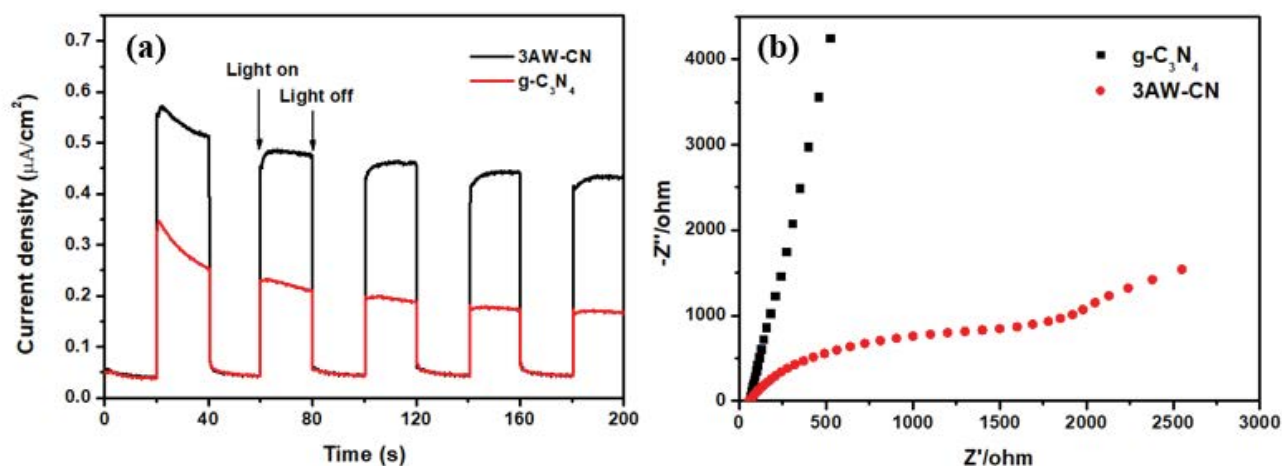


Fig. 9. Transient photocurrent responses (a) and EIS Nyquist plots of  $g\text{-C}_3\text{N}_4$  and 3AW-CN (b).

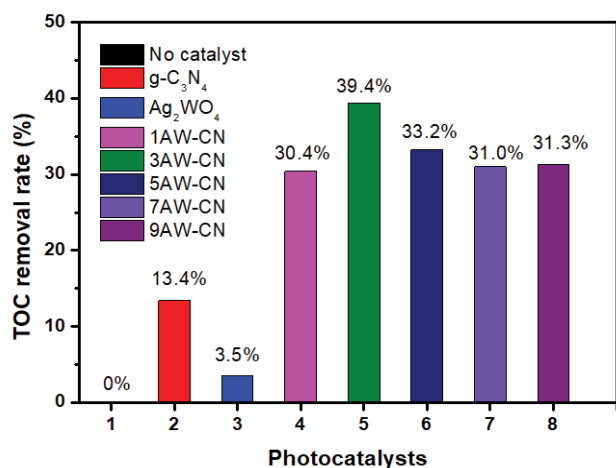


Fig. 10. Removal rates of TOC from TC solutions within 180 min by using the photocatalyst.

Hence, the possible mechanism for photocatalytic degradation of TC by 3AW-CN heterojunction photocatalyst under visible light is proposed in Fig. 11.

According to the formula:  $E_{\text{VB}} = X - E_{\text{C}} + 1/2 E_{\text{g}}$  [35], the valence band positions of pure  $g\text{-C}_3\text{N}_4$  and pure  $\text{Ag}_2\text{WO}_4$  are calculated to be 1.71 and 3.11 eV, respectively.

In the light of the band gap (Fig. 6b), the conduction band of  $g\text{-C}_3\text{N}_4$  and  $\text{Ag}_2\text{WO}_4$  locates at  $-0.99$  and  $0.04$  eV, respectively. Obviously, the conduction band of  $\text{Ag}_2\text{WO}_4$  is more positive than that of  $g\text{-C}_3\text{N}_4$ , indicating that the potentials of  $g\text{-C}_3\text{N}_4$  and  $\text{Ag}_2\text{WO}_4$  can match and form an AW-CN heterojunction, so the possible charge separation and transfer mechanisms may exist as follows:

$g\text{-C}_3\text{N}_4$  absorbs visible-light and was excited to produce photogenerated electrons, leaving corresponding photogenerated holes on the valence band. At the same time,  $\text{Ag}^+$  is reduced to Ag nanoparticles under illumination, and then Ag nanoparticles absorb visible-light and generate electrons due to SPR effect [51]. As the electron reservoir and donor, Ag nanoparticles can transfer electrons to the conduction

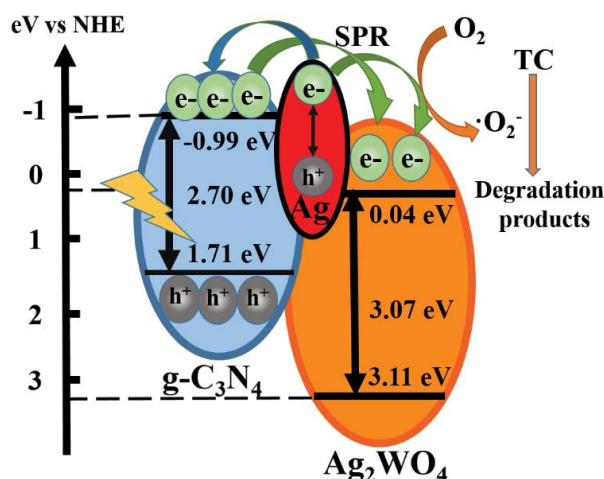


Fig. 11. Possible photocatalytic degradation mechanisms of TC by 3AW-CN heterojunction.

band of  $g\text{-C}_3\text{N}_4$  and  $\text{Ag}_2\text{WO}_4$ . Finally, the electrons on the conduction band of  $g\text{-C}_3\text{N}_4$  ( $-0.99$  eV) are transferred to the more positive position of the  $\text{Ag}_2\text{WO}_4$  conduction band ( $0.04$  eV) for reacting with oxygen molecules in water to produce  $\text{O}_2^-$  during the transferring process, and the holes on the valence band of  $g\text{-C}_3\text{N}_4$  is used to decompose TC. Therefore,  $\text{O}_2^-$  and holes are the main active species, which is consistent with the results of active species trapping experiment of the 3AW-CN heterojunction.

Overall, heterojunction photocatalyst  $\text{Ag}_2\text{WO}_4/g\text{-C}_3\text{N}_4$  can quickly and effectively separate photogenerated electron-holes, and then a large number of  $\text{O}_2^-$  was induced to be generated to participate in the photocatalytic degradation reaction of TC. Finally, TC is effectively removed.

#### 4. Conclusions

In summary,  $\text{Ag}_2\text{WO}_4/g\text{-C}_3\text{N}_4$  heterojunction photocatalyst which contains a small quantity of  $\text{Ag}_2\text{WO}_4$  is successfully

synthesized by a simple precipitation method. Compared with pure g-C<sub>3</sub>N<sub>4</sub> and pure Ag<sub>2</sub>WO<sub>4</sub>, AW-CN can significantly enhance the photocatalytic degradation activity of tetracycline (TC) under visible-light irradiation. Especially, 3AW-CN shows the highest photocatalytic degradation efficiency of TC (76.9%, 180 min).

The improvement of photocatalytic activity is due to three aspects: first, the deposition of Ag<sub>2</sub>WO<sub>4</sub> enhances the absorption of visible-light by g-C<sub>3</sub>N<sub>4</sub>; second, the heterojunction effectively inhibits the recombination of photogenerated electron-hole pair; at last, as the reservoir and donor of electrons, silver nanoparticles can effectively regulate the transfer of electrons to the conduction band of Ag<sub>2</sub>WO<sub>4</sub>, thus accelerating the photodegradation reaction.

### Acknowledgement

This work was supported by Zhangjiagang Science and Technology Support Program (Social Development) of Jiangsu Province, China (grant number: ZKS1510).

### References

- [1] Z. Cetecioglu, B. Ince, M. Gros, S. Rodriguez-Mozaz, D. Barceloe, D. Orhon, O. Ince, Chronic impact of tetracycline on the biodegradation of an organic substrate mixture under anaerobic conditions, *Water Res.*, 47 (2013) 2959–2969.
- [2] R. Daghrir, P. Drogui, Tetracycline antibiotics in the environment: a review, *Environ. Chem. Lett.*, 11 (2013) 209–227.
- [3] N. Pastor-Navarro, A. Maquieira, R. Puchades, Review on immunoanalytical determination of tetracycline and sulfonamide residues in edible products, *Anal. Bioanal. Chem.*, 395 (2009) 907–920.
- [4] R. Asahi, T. Morikawa, T. Ohwaki, K. Aoki, Y. Taga, Visible-light photocatalysis in nitrogen-doped titanium oxides, *Science*, 293 (2001) 269–271.
- [5] J. Wang, P. Zhang, X. Li, J. Zhu, H. Li, Synchronical pollutant degradation and H<sub>2</sub> production on a Ti<sup>3+</sup>-doped TiO<sub>2</sub> visible photocatalyst with dominant (001) facets, *Appl. Catal., B*, 134–135 (2013) 198–204.
- [6] J. Tian, Y.H. Sang, Z.H. Zhao, W.J. Zhou, D.Z. Wang, X.L. Kang, H. Liu, J.Y. Wang, S.W. Chen, H.Q. Cai, H. Huang, Enhanced photocatalytic performances of CeO<sub>2</sub>/TiO<sub>2</sub> nanobelt heterostructures, *Small*, 9 (2013) 3864–3872.
- [7] O. Carp, C.L. Huisman, A. Reller, Photoinduced reactivity of titanium dioxide, *Prog. Solid State Chem.*, 32 (2004) 33–177.
- [8] O. Ola, M.M. Maroto-Valer, Review of material design and reactor engineering on TiO<sub>2</sub> photocatalysis for CO<sub>2</sub> reduction, *J. Photochem. Photobiol. C*, 24 (2015) 16–42.
- [9] Y.H. Song, H.Z. Zhao, Z.G. Chen, W.R. Wang, L.Y. Huang, H. Xu, H.M. Li, The CeO<sub>2</sub>/Ag<sub>3</sub>PO<sub>4</sub> photocatalyst with stability and high photocatalytic activity under visible light irradiation, *Phys. Status Solidi A*, 213 (2016) 2356–2363.
- [10] W. Teng, X.J. Tan, X.Y. Li, Y.B. Tang, Novel Ag<sub>3</sub>PO<sub>4</sub>/MoO<sub>3</sub> p-n heterojunction with enhanced photocatalytic activity and stability under visible light irradiation, *Appl. Surf. Sci.*, 409 (2017) 250–260.
- [11] W.L. Shi, F. Guo, M.Y. Li, Y. Shi, M.J. Shi, C. Yan, Constructing 3D sub-micrometer CoO octahedrons packed with layered MoS<sub>2</sub> shell for boosting photocatalytic overall water splitting activity, *Appl. Surface Sci.*, 473 (2019) 928–933.
- [12] R.B. Wei, Z.L. Huang, G.H. Gu, Z. Wang, L.X. Zeng, Y.B. Chen, Z.Q. Liu, Dual-cocatalysts decorated rimous CdS spheres advancing highly-efficient visible-light photocatalytic hydrogen production, *Appl. Catal., B*, 231 (2018) 101–107.
- [13] J.B. Sun, J.R. Song, M.A. Gondal, S. Shi, Z.X. Lu, Q.Y. Xu, X.F. Chang, D.H. Xiang, K. Shen, Preparation of g-C<sub>3</sub>N<sub>4</sub>/BiOX (X = Cl, Br, I) composites, and their photocatalytic activity under visible light irradiation, *Res. Chem. Intermed.*, 41 (2015) 6941–6955.
- [14] Y.B. Tang, H.J. Yang, F.Y. Chen, X.G. Wang, Preparation, characterization of nanocomposites plasmonic photocatalyst C@ (Fe<sub>3</sub>O<sub>4</sub>-halloysite nanotubes)-Ag/AgCl and its photocatalytic activity, *Desal. Wat. Treat.*, 110 (2018) 144–153.
- [15] J.X. Yu, Q.Y. Nong, X.L. Jiang, X.Z. Liu, Y. Wu, Y.M. He, Novel Fe<sub>2</sub>(MoO<sub>4</sub>)<sub>3</sub>/g-C<sub>3</sub>N<sub>4</sub> heterojunction for efficient contaminant removal and hydrogen production under visible light irradiation, *Sol. Energy*, 139 (2016) 355–364.
- [16] Y.G. Zhou, Y.F. Zhang, M.S. Lin, J.L. Long, Z.Z. Zhang, H.X. Lin, C. Jeffrey, S. Wu, X.X. Wang, Monolayered Bi<sub>2</sub>WO<sub>6</sub> nanosheets mimicking heterojunction interface with open surfaces for photocatalysis, *Nat. Commun.*, 6 (2015) 8340.
- [17] S.Y. Song, Y. Zhang, Y. Xing, C. Wang, J. Feng, W.D. Shi, G.L. Zhang, H.J. Zhang, Rectangular AgIn(WO<sub>4</sub>)<sub>2</sub> nanotubes: a promising photoelectric material, *Adv. Funct. Mater.*, 18 (2008) 2328–2334.
- [18] L.B. Jiang, X.Z. Yuan, G.M. Zeng, J. Liang, Z.B. Wu, H. Wang, J. Zhang, T. Xiong, H. Lic, A facile band alignment of polymeric carbon nitride isotype heterojunctions for enhanced photocatalytic tetracycline degradation, *Environ. Sci.: Nano*, 5 (2018) 2604–2617.
- [19] L.B. Jiang, X.Z. Yuan, G.M. Zeng, J. Liang, Z.B. Wu, H.B. Yu, D. Mo, H. Wang, Z.H. Xiao, C.Y. Zhou, Nitrogen self-doped g-C<sub>3</sub>N<sub>4</sub> nanosheets with tunable band structures for enhanced photocatalytic tetracycline degradation, *J. Colloid Interface Sci.*, 536 (2019) 17–29.
- [20] Y. Yu, W. Yan, X.F. Wang, P. Li, W.Y. Gao, H.H. Zou, S.M. Wu, K.J. Ding, Surface engineering for extremely enhanced charge separation and photocatalytic hydrogen evolution on g-C<sub>3</sub>N<sub>4</sub>, *Adv. Mater.*, 30 (2018) 1705060.
- [21] L.B. Jiang, X.Z. Yuan, Y. Pan, J. Liang, G.M. Zeng, Z.B. Wu, H. Wang, Doping of graphitic carbon nitride for photocatalysis: s review, *Appl. Catal., B*, 217 (2017) 388–406.
- [22] Y.J. Cui, Y.B. Tang, X.C. Wang, Template-free synthesis of graphitic carbon nitride hollow spheres for photocatalytic degradation of organic pollutants, *Mater. Lett.*, 161 (2015) 197–200.
- [23] L.B. Jiang, X.Z. Yuan, G.M. Zeng, J. Liang, Z.B. Wu, H. Wang, Construction of all-solid-state Z-scheme photocatalyst based on graphite carbon nitride and its enhancement to catalytic activity, *Environ. Sci.: Nano*, 10 (2018) 599–615.
- [24] L. Ma, G.H. Wang, C.J. Jiang, H.L. Bao, Synthesis of core-shell TiO<sub>2</sub>@g-C<sub>3</sub>N<sub>4</sub> hollow microspheres for efficient photocatalytic degradation of rhodamine B under visible light, *Appl. Surf. Sci.*, 430 (2018) 263–272.
- [25] L.B. Jian, X.Z. Yuan, G.M. Zeng, J. Liang, X.H. Chen, H.B. Yu, H. Wang, Z.B. Wu, J. Zhang, T. Xiong, In-situ synthesis of direct solid-state dual Z-scheme WO<sub>3</sub>/g-C<sub>3</sub>N<sub>4</sub>/Bi<sub>2</sub>O<sub>3</sub> photocatalyst for the degradation of refractory pollutant, *Appl. Catal., B*, 227 (2018) 376–385.
- [26] P.F. Xia, B.C. Zhu, B. Cheng, J.G. Yu, 2D/2D g-C<sub>3</sub>N<sub>4</sub>/MnO<sub>2</sub> nanocomposite as a direct Z-scheme photocatalyst for enhanced photocatalytic activity, *ACS Sustain. Chem. Eng.*, 6 (2018) 965–973.
- [27] A. Akhundi, A. Habibi-Yangjeh, Novel g-C<sub>3</sub>N<sub>4</sub>/Ag<sub>2</sub>SO<sub>4</sub> nanocomposites: fast microwave-assisted preparation and enhanced photocatalytic performance towards degradation of organic pollutants under visible light, *Colloid Interface Sci.*, 482 (2016) 165–174.
- [28] Y. Gong, X. Quan, H.T. Yu, S. Chen, Synthesis of Z-scheme Ag<sub>2</sub>CrO<sub>4</sub>/Ag/g-C<sub>3</sub>N<sub>4</sub> composite with enhanced visible-light photocatalytic activity for 2,4-dichlorophenol degradation, *Appl. Catal., B*, 219 (2017) 439–449.
- [29] A. Akhundi, A. Habibi-Yangjeh, High performance magnetically recoverable g-C<sub>3</sub>N<sub>4</sub>/Fe<sub>3</sub>O<sub>4</sub>/Ag/Ag<sub>2</sub>SO<sub>3</sub> plasmonic photocatalyst for enhanced photocatalytic degradation of water pollutants, *Adv. Powder Technol.*, 28 (2017) 565–574.
- [30] S.L. Ma, S.H. Zhan, Y.N. Jia, Q. Shi, Q.X. Zhou, Enhanced disinfection application of Ag-modified g-C<sub>3</sub>N<sub>4</sub> composite under visible light, *Appl. Catal., B*, 186 (2016) 77–87.

- [31] Z. Zhu, Z.Y. Lu, D.D. Wang, X. Tang, Y.S. Yan, W.D. Shi, Y.S. Wang, N.L. Gao, X. Yao, H.J. Dong, Construction of high-dispersed Ag/Fe<sub>3</sub>O<sub>4</sub>/g-C<sub>3</sub>N<sub>4</sub> photocatalyst by selective photo-deposition and improved photocatalytic activity, *Appl. Catal., B*, 182 (2016) 115–122.
- [32] J.Y. Qin, J.P. Huo, P.Y. Zhang, J. Zeng, T.T. Wang, H.P. Zeng, Improving the photocatalytic hydrogen production of Ag/g-C<sub>3</sub>N<sub>4</sub> nanocomposites by dye-sensitization under visible light irradiation, *Nanoscale*, 8 (2016) 2249–2259.
- [33] Y.M. He, L.H. Zhang, B.T. Teng, M.H. Fan, New application of Z-scheme Ag<sub>3</sub>PO<sub>4</sub>/g-C<sub>3</sub>N<sub>4</sub> composite in converting CO<sub>2</sub> to fuel, *Environ. Sci. Technol.*, 49 (2015) 649–656.
- [34] W.J. Ong, L.K. Putri, L.L. Tan, S.P. Chai, S.T. Yong, Heterostructured AgX/g-C<sub>3</sub>N<sub>4</sub> (X = Cl and Br) nanocomposites via a sonication-assisted deposition-precipitation approach: emerging role of halide ions in the synergistic photocatalytic reduction of carbon dioxide, *Appl. Catal., B*, 180 (2016) 530–543.
- [35] Y.J. Wang, Y.M. He, T.T. Li, J. Cai, M.F. Luo, L.H. Zhao, Photocatalytic degradation of methylene blue on CaBi<sub>6</sub>O<sub>10</sub>/Bi<sub>2</sub>O<sub>3</sub> composites under visible light, *Chem. Eng. J.*, 189–190 (2012) 473–481.
- [36] K. Dai, J.L. Lv, L.H. Lu, C.H. Liang, L. Geng, G.P. Zhu, A facile fabrication of plasmonic g-C<sub>3</sub>N<sub>4</sub>/Ag<sub>2</sub>WO<sub>4</sub>/Ag ternary heterojunction visible-light photocatalyst, *Mater. Chem. Phys.*, 177 (2016) 529–537.
- [37] X.L. Jiang, X.Z. Liu, Q.Q. Chen, R.S. Jin, Y. Lu, J.X. Yu, Y. Wu, Y.M. He, Preparation and photocatalytic activity of an inorganic-organic hybrid photocatalyst Ag<sub>2</sub>WO<sub>4</sub>/g-C<sub>3</sub>N<sub>4</sub>, *J. Inorg. Organomet. Polym. Mater.*, 27 (2017) 1683–1693.
- [38] F. Goettmann, A. Fischer, M. Antonietti, A. Thomas, Chemical synthesis of mesoporous carbon nitrides using hard templates and their use as a metal-free catalyst for Friedel-Crafts reaction of benzene, *Angew. Chem. Int. Edit.*, 45 (2006) 4467–4471.
- [39] X.J. Bai, R.L. Zong, C.X. Li, D. Liu, Y.F. Liu, Y.F. Zhu, Enhancement of visible photocatalytic activity via Ag@C<sub>3</sub>N<sub>4</sub> core-shell plasmonic composite, *Appl. Catal., B*, 147 (2014) 82–91.
- [40] B.C. Zhu, P.F. Xia, Y. Li, W.K. Ho, J.G. Yu, Fabrication and photocatalytic activity enhanced mechanism of direct Z-scheme g-C<sub>3</sub>N<sub>4</sub>/Ag<sub>2</sub>WO<sub>4</sub> photocatalyst, *Appl. Surf. Sci.*, 391 (2017) 175–183.
- [41] Y. Li, Y.N. Li, S.L. Ma, P.F. Wang, Q.L. Hou, J.J. Han, S.H. Zhan, Efficient water disinfection with Ag<sub>2</sub>WO<sub>4</sub>-doped mesoporous g-C<sub>3</sub>N<sub>4</sub> under visible light, *Hazard. Mater.*, 338 (2017) 33–46.
- [42] M.H. Habibi, P. Bagheri, Enhanced photo-catalytic degradation of naphthol blue black on nano-structure MnCo<sub>2</sub>O<sub>4</sub>: charge separation of the photo-generated electron-hole pair, *Mater. Sci. Mater. El.*, 28 (2017) 289–294.
- [43] L. Ge, C.C. Han, Synthesis of MWNTs/g-C<sub>3</sub>N<sub>4</sub> composite photocatalysts with efficient visible light photocatalytic hydrogen evolution activity, *Appl. Catal., B*, 117–118 (2012) 268–274.
- [44] Y.S. Fu, T. Huang, B.Q. Jia, J.W. Zhu, X. Wang, Reduction of nitrophenols to aminophenols under concerted catalysis by Au/g-C<sub>3</sub>N<sub>4</sub> contact system, *Appl. Catal., B*, 202 (2017) 430–437.
- [45] Y. Wu, H. Wang, W.G. Tu, Y. Liu, S.Y. Wu, Y.Z. Tan, J.W. Chew, Construction of hierarchical 2D-2D Zn<sub>3</sub>In<sub>2</sub>S<sub>6</sub>/fluorinated polymeric carbon nitride nanosheets photocatalyst for boosting photocatalytic degradation and hydrogen production performance, *Appl. Catal., B*, 233 (2018) 58–69.
- [46] Y.F. Li, R.X. Jin, X. Fang, Y. Yang, M. Yang, X.C. Liu, Y. Xing, S.Y. Song, In situ loading of Ag<sub>2</sub>WO<sub>4</sub> on ultrathin g-C<sub>3</sub>N<sub>4</sub> nanosheets with highly enhanced photocatalytic performance, *J. Hazard. Mater.*, 313 (2016) 219–228.
- [47] W.L. Shi, F. Guo, M.Y. Li, Y. Shi, M.F. Wu, Y.B. Tang, Enhanced visible-light-driven photocatalytic H<sub>2</sub> evolution on the novel nitrogen-doped carbon dots/CuBi<sub>2</sub>O<sub>4</sub> microrods composite, *J. Alloys Comp.*, 775 (2019) 511–517.
- [48] G. Liu, P. Niu, C.H. Sun, S.C. Smith, Z.G. Chen, G. Lu, H.M. Cheng, Unique electronic structure induced high photo-reactivity of sulfur-doped graphitic C<sub>3</sub>N<sub>4</sub>, *J. Am. Chem. Soc.*, 132 (2010) 11642–11648.
- [49] C. Karunakaran, S. Kalaiivani, P. Vinayagamorthy, S. Dash, Electrical, optical and visible light-photocatalytic properties of

monoclinic BiVO<sub>4</sub> nanoparticles synthesized hydrothermally at different pH, *Mater. Sci. Semicond. Proc.*, 21 (2014) 122–131.

- [50] C.M. Li, S.Y. Yu, X.X. Zhang, Y. Wang, C.B. Liu, G. Chen, H.J. Dong, Insight into photocatalytic activity, universality and mechanism of copper/chlorine surface dual-doped graphitic carbon nitride for degrading various organic pollutants in water, *Colloid Interface Sci.*, 538 (2019) 462–473.
- [51] L.G. Devi, R. Kavitha, A review on plasmonic metal-TiO<sub>2</sub> composite for generation, trapping, storing and dynamic vectorial transfer of photogenerated electrons across the Schottky junction in a photocatalytic system, *Appl. Surf. Sci.*, 360 (2016) 601–622.

## Supporting information:

### S1. Structural characterization

X-ray diffraction patterns of materials prepared were recorded using an X'Pert-Pro MPD (Holand) D/max-γA X-ray diffractometer with Cu Kα radiation ( $\lambda = 0.154178$  nm). High-resolution transmission electron microscope was performed with an FEI-Tecna F20 microscope operating at 200 kV, respectively. X-ray photoelectron spectroscopy (XPS) was carried out on a KRATOS Axis ultra-DLD X-ray photoelectron spectrometer with a monochromatic Al Kα X-ray source. UV–vis absorption spectra of the samples were recorded on a UV–Vis spectrophotometer (UV-2550, Shimadzu Instrument Co. Ltd., Japan) in the tested range of 200–800 nm. Photoluminescence (PL) spectra of the as-prepared samples were detected by Fluorolog-TCSPEC luminescence spectrometer. The photocurrent–time (*i-t*) curves and electrochemical impedance spectroscopy (EIS) measurements were performed on a CHI 920C workstation (CH Instruments, Chenhua, Shanghai, China) using a standard three-electrode cell with a platinum wire as reference electrode and a saturated calomel electrode as counter electrode. The *i-t* curves were gained at open circuit potential in 0.1 M Na<sub>2</sub>SO<sub>4</sub> electrolyte and a 300 W Xenon lamp with UV–Vis-cutoff filter ( $\lambda > 420$  nm) was used as the visible-light source. The EIS was recorded by using an alternating voltage of 5 mV amplitude in the frequency range of 10<sup>5</sup> to 10<sup>2</sup> Hz.

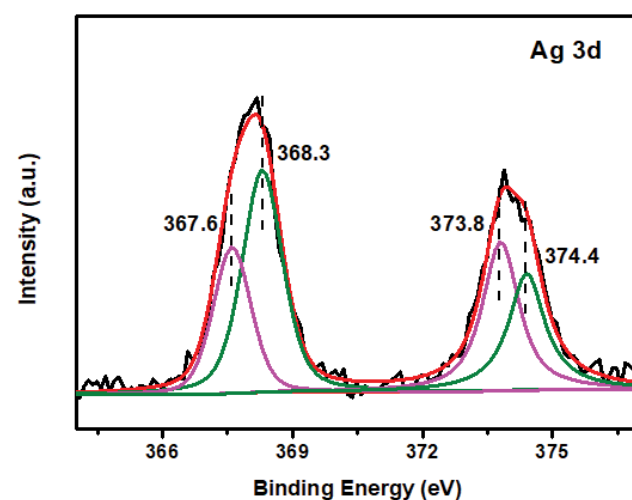


Fig. S1. XPS spectrum of Ag 3d in the 3AW-CN sample after one experiment.

Total organic carbons (TOC) were measured on a multi N/C 2100 (Analytik Jena AG, Germany) TOC analyzer.

## S2. Photocatalytic degradation experiment

The photocatalytic activity of g-C<sub>3</sub>N<sub>4</sub> structure and its hybrid composites Ag<sub>2</sub>WO<sub>4</sub>/g-C<sub>3</sub>N<sub>4</sub> was investigated for TC degradation without adjusting the pH. A 150 W Xenon arc lamp simulated solar light with intensity 100 mW cm<sup>-2</sup> was used as a visible-light source.

100 mL of TC aqueous solutions (10 mg/L) was taken into a 200 mL beaker and 50 mg of the catalyst was added at each cycle runs. Throughout the experiments, the TC aqueous solution was maintained at a distance of 15 cm away from the light source.

The solution was stirred under the dark condition for 30 min before irradiation in order to obtain the adsorption-desorption equilibrium.

The degradation of TC was analyzed by UV–visible spectrophotometer ( $\lambda_{\text{max}}$  of TC = 357 nm) at a regular time intervals, and, 5 mL of the samples were taken each time. After centrifugation, the supernate was examined using spectroscopy analysis and the changes in absorption vs. irradiation time ( $C/C_0$  vs.  $t$ ) were recorded.

The photodegradation percentage of TC was calculated using the formula as follows:

$$\text{Photodegradation (\% of TC)} = [(C_0 - C)/C_0] \quad (S1)$$

where,  $C_0$  is the concentration of TC aqueous solutions before irradiation and  $C$  is the concentration of TC aqueous solutions after a particular period of irradiation time.